The Trimerization Domain of Nemo Is Composed of the Interacting C-terminal CC2 and LZ Coiled-coil Subdomains

Fabrice Agou, François Traincard, Emilie Vinolo, Gilles Courtois, Shoji Yamaoka, Alain Israël, Michel Véron

THE JOURNAL OF BIOLOGICAL CHEMISTRY
Vol. 279, No. 27, Issue of July 2, pp. 27861–27869, 2004
Printed in U.S.A.

The Trimerization Domain of Nemo Is Composed of the Interacting C-terminal CC2 and LZ Coiled-coil Subdomains*

Received for publication, December 30, 2003, and in revised form, April 23, 2004
Published, JBC Papers in Press, April 23, 2004, DOI 10.1074/jbc.M314278200

Fabrice Agou‡§, François Traincard‡, Emilie Vinolo‡, Gilles Courtois¶, Shoji Yamaoka¶‖, Alain Israël¶, and Michel Véron‡

From the ‡Unité de Régulation Enzymatique des Activités Cellulaires, CNRS URA 2185 and the ¶Unité de Biologie Moléculaire de l'Expression Génique, CNRS URA 2582, Institut Pasteur, 25 rue du Dr Roux, 75724 Paris Cedex 15, France and the ‖Department of Microbiology, Tokyo Medical and Dental University, School of Medicine, Yushima 1-5-45 Bunkyo-ku, Tokyo, Japan

NEMO (NF-κB essential modulator) plays a key role in the canonical NF-κB pathway as the scaffold/regulatory component of the IκB kinase (IKK) complex. The self-association of NEMO involves the C-terminal halves of the polypeptide chains containing two putative coiled-coil motifs (a CC2 and a LZ leucine zipper), a proline-rich region, and a ZF zinc finger motif. Using purified truncation mutants, we showed that the minimal oligomerization domain of NEMO is the CC2-LZ segment and that both CC2 and LZ subdomains are necessary to restore the LPS-dependent activation of the NF-κB pathway in a NEMO-deficient cell line. We confirmed the association of the oligomerization domain in a trimer and investigated the specific role of CC2 and LZ subdomains in the building of the oligomer. Whereas a recombinant CC2-LZ polypeptide self-associated into a trimer with an association constant close to that of the wild-type protein, the isolated CC2 and LZ peptides, respectively, formed trimers and dimers with weaker association constants. Upon mixing, isolated CC2 and LZ peptides associated to form a stable hetero-hexamer as shown by gel filtration and fluorescence anisotropy experiments. We propose a structural model for the organization of the oligomerization domain of activated NEMO in which three C-terminal domains associate into a pseudo-hexamer forming a six-helix bundle. This model is discussed in relation to the mechanism of activation of the IKK complex by upstream activators.

The NF-κB signaling pathway plays a central role in the regulation of gene expression pertaining to inflammation, the immune response, oncogenesis, and apoptosis (1–5). In this canonical pathway, pro-inflammatory stimuli promote NF-κB activation via phosphorylation of IκB inhibitors by the kinases of the IKK[1] complex. This phosphorylation is in turn followed by ubiquitination and degradation of IκB by the proteasome, allowing the NF-κB transcription factors to enter the nucleus and to activate their target genes (4).

The IKK complex contains two protein kinases, IKK-α and IKK-β, and a structural/regulatory subunit called NEMO (NF-κB essential modulator) or IKK-γ (6–8). NEMO is the key regulator of the NF-κB pathway as genetic inactivation abolishes signaling in response to several extracellular stimuli (6, 9, 10). The activation of IKK-β is mediated through the *trans*-phosphorylation between IKK kinases (11). The mechanism by which NEMO is activated remains unclear and several factors have been proposed to be involved, including phosphorylation (12) and ubiquitination (13). Indeed, the de-ubiquitinating enzyme CYLD negatively regulates NF-κB activation by specific tumor-necrosis factor receptors (14, 15) and was recently shown to de-ubiquitinate NEMO (15, 16). Converging evidence suggests that NEMO oligomerization plays a crucial role in the activation of the IKK complex. Indeed, IKK can be activated by the enforced oligomerization of NEMO through the fusion with the FKBP12 polypeptide (17, 18) or through oligomerization of the equine herpes virus-2 vCLAP protein, a NEMO-binding protein (19). In addition, the binding of Tax, a well known NF-κB activator, to NEMO also results in its oligomerization (20).

The quaternary structure of NEMO is a matter of debate. *In vitro* cross-linking experiments with the non-cleavable amine-reactive bis(sulfosuccinimidyl)suberate cross-linker established that pure recombinant NEMO autoassociates in dimers and trimers (20). Using a very similar amine-reactive cross-linking agent, ethylene glycol-bissuccinimidylsuccinate, Rothwarf *et al.* (7) also found dimeric and trimeric forms of recombinant NEMO. In contrast, when using the same broad spectrum cross-linking reagent in crude extracts from HeLa cells, Tegethoff *et al.* (21) reported that NEMO predominantly forms tetramers. In our laboratory, we used bis(maleimido)ethane, a cell-permeable cysteine cross-linker, to show that NEMO associates into both dimers and trimers in HeLa cells (1) as well as in MCF-7 and MDA-MB-435S cells.[2] We also showed, using gel filtration and sedimentation equilibrium, that the purified C-terminal domain of NEMO (amino acids 242–388)[3] (hereafter called the C-ter domain) self-assembles into trimers (1).

A "minimal oligomerization domain" has been identified within this C-ter domain based on immunoprecipitation assays and functional complementation assays (21). This minimal domain corresponds to amino acids 246–365. The NEMO C-ter domain contains three predicted structural motifs (see Fig. 2):

* This work was supported by grants from the Association pour la Recherche sur le Cancer (ARC number 5795) and the Ligue Nationale contre le Cancer (équipe labelisée) (to A. I.). The costs of publication of this article were defrayed in part by the payment of page charges. This article must therefore be hereby marked "*advertisement*" in accordance with 18 U.S.C. Section 1734 solely to indicate this fact.

§ To whom correspondence should be addressed. Tel.: 33-1-45-68-83-80; Fax: 33-1-45-68-83-99; E-mail: fagou@pasteur.fr.

[1] The abbreviations used are: IKK, IκB kinase; DDM, *n*-dodecylmaltoside; GdmCl, guanidinium chloride; HA, hemagglutinin tag; wt, wild-type; IL, interleukin; LZ, leucine zipper; ZF, zinc finger; IκB, inhibitor of κB; sp, synthetic peptide; NEMO, NF-κB essential modulator; MES, 4-morpholineethanesulfonic acid; Fmoc, *N*-(9-fluorenyl)methoxycarbonyl; C-ter, C-terminal domain; EMSA, electrophoretic mobility shift assay; LPS, lipopolysaccharide.

[2] F. Agou, unpublished results.

[3] In this report amino acid numbering refers to the mouse sequence.

a coil-coiled motif (CC2) (amino acids 253–285, murine sequence), a leucine zipper (LZ) (amino acids 301–337), and a zinc finger motif (ZF) at the extreme C terminus of the protein (amino acids 389–410). The ZF motif is required for UV-induced NF-κB activation (22) and for the response to tumor necrosis factorα or interleukin-1.[4] Mutations in this C-ter domain result in two human diseases, incontinentia pigmenti and anhidrotic ectodermal dysplasia with immunodeficiency (23–25). The discovery of two mutations in patients with anhidrotic ectodermal dysplasia with immunodeficiency suggests that the oligomerization state of NEMO plays a role in the pathological defects of the NF-κB signal transduction pathway. Interestingly, D304N is located in the predicted α helix that is upstream from the canonical LZ motif beginning at Leu^{315}, and A281G is in the CC2 motif (24).

In this report, we investigated the functional and structural roles of the subdomains constituting the C-ter domain of NEMO. We used gel filtration and sedimentation equilibrium to compare the assembly properties of several highly purified truncated proteins containing a combination of CC2, LZ, and ZF motifs. We show that the minimal oligomerization domain of NEMO consists of the CC2 and LZ coiled-coils, and that these subdomains can interact to form a highly stable pseudohexameric structure. On the basis of these results, we propose a structural model for the C-terminal domain of NEMO.

EXPERIMENTAL PROCEDURES

Reagents—Anti-His tag antibodies were from Qiagen, octyl glucoside and dodecyl maltoside were from Roche Molecular Biochemicals, Geneticin (G418) was from Invitrogen, and anti-NEMO polyclonal antibody was prepared as described previously (6).

Functional Complementation of 1.3E2 Cells—An HA-tagged murine NEMO expression vector, *HA-nemo*, was constructed by inserting a PCR-amplified *nemo* cDNA into pcDNA3-HA, a modified version of pcDNA3 (Invitrogen). The sequences of the primers used for PCR amplification were: 5′-GCGCGTCGACAACAAGCACCCCTGGAAG-3′ and 5′-GGGCGCTAGCTAATCACCGGGAAGAAAGGTAC-3′. The PCR product was digested with SalI and XbaI and cloned into XhoI/XbaI-digested pcDNA3-HA. *HA-LZ-mut-nemo* was constructed by inserting a PCR-amplified *nemo* cDNA fragment produced by an overlapping PCR method into pcDNA3-HA. The sequences of the primers used for the first PCR amplification step were: 5′-GCGCGTCGACAACAAGCACCCCTGGAAG-3′, 5′-GTTGAACTCGCGCTGCGACTGCTCCAGCTGCTCCTGCGAATACTCCTTCTTCTC-3, 5′-GAGAAGAAGGAGTATTCGCAGGAGCAGCTGGAGCAGTCGCAGCGCGAGTTCAAC-3′, and 5′-GGGCGCTAGCTAATCACCGGGAAGAAAGGTAC-3′ (mutations are underlined). Each PCR product was purified, mixed with each other, and subjected to a few additional cycles of PCR in the absence of primers. The products were then subjected to a third PCR using: 5′-GCGCGTCGACAACAAGCACCCCTGGAAG-3′ and 5′-GGGCGCTAGCTAATCACCGGGAAGAAAGGTAC-3′. The PCR product was digested with SalI and XbaI and cloned into XhoI/XbaI-digested pcDNA3-HA, generating a HA-NEMO that contained a S322A/S329A double mutation (LZ mut).

HA-ΔCC2-nemo, encoding an HA-tagged NEMO lacking amino acids 280–311, was prepared by using pBX-*nemo*, a pBluescript-derivative containing a BamHI/XbaI fragment of *nemo* isolated from *HA-nemo*. pBX-*nemo* was digested with AvaI, filled in with the Klenow fragment, digested with SphI, and treated with T4 DNA polymerase. After self-ligation, the resulting 4.2-kb fragment was digested with BamHI and XbaI, and the recovered 1.4-kb fragment was cloned into pcDNA3-HA.

Stable and Transient Transfections—The 1.3E2 cells were transiently transfected essentially as in a previous study (26). To generate stable 1.3E2 clones, 5 μg of *HA-nemo* or *HA-LZ-mut-nemo* plasmids were added to 5×10^6 cells in a 500-μl volume and electroporated at 260 V, 1500 microfarads, and R ∞. G418 (1 μg/ml) was added the following day, and cells were cloned by limited dilution after a week of selection. Expression of HA-NEMO was checked using the anti-HA antibody. Transfected clones expressing NEMO at a level similar to parental 70Z/3 cells were selected for further analysis.

[4] S. Yamaoka, unpublished results.

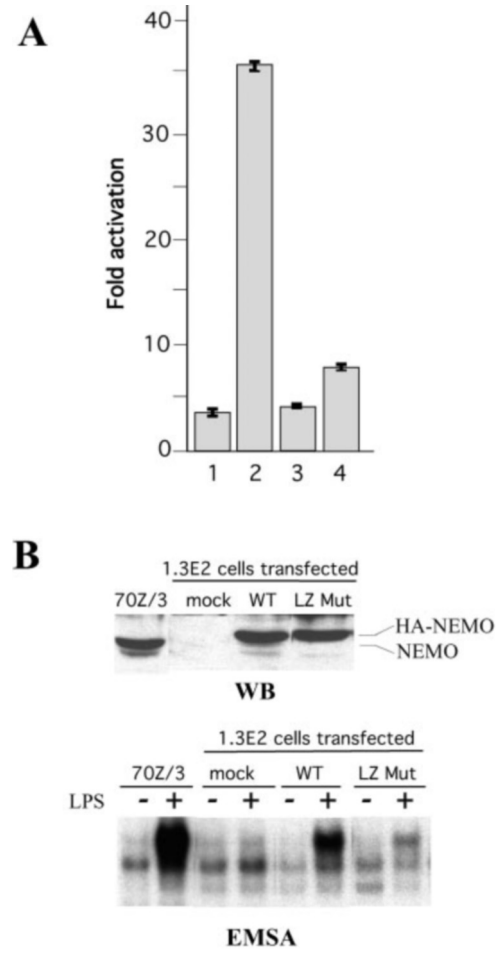

FIG. 1. **Functional complementation of 1.3E2 cells.** *A*, transient transfections. 1.3E2 cells were co-transfected with the reporter plasmid Igκ-luciferase and either mock transfected (*1*) or transfected with a plasmid bearing *Nemo* wt cDNA (*2*), *nemo* cDNA deleted of part of the CC2 motif (*3*), or *nemo* cDNA carrying the double mutation L322S/L329S in the LZ motif (*4*). The activation of the NF-κB pathway by LPS is expressed as the ratio of luciferase activity in cell extracts in the presence and absence of LPS. *B*, stable transfection. Western blot (*WB*) of NEMO expression levels in cell extracts. 1.3E2 cells were either mock transfected or transfected with a wt *nemo* cDNA or transfected with the L322S/L349S mutant (*LZ Mut*). Gel retardation assays (EMSA) of nuclear extracts from resting (−) and LPS-activated (+) cells (lanes as above). WB and EMSA performed with the parental 70Z/3 cells (*70Z/3*) are also shown. *HA-NEMO*, HA-tagged NEMO protein; *NEMO*, endogenous NEMO.

Peptide Synthesis and Purification—Peptides were synthesized on an Applied Biosystems (Foster City, CA) Pioneer peptide synthesizer by continuous flow Fmoc/ter-butyl chemistry (27) and purified as described previously (28). All peptides were blocked with an acetyl group at their N terminus and with an amide at their C terminus. Purified peptides were quantified by amino acid analysis and characterized by positive ion electrospray ionization mass spectrometry before storage at −20 °C at a concentration of 2 mM in water. The following peptides were synthesized: sp-CC2 (^{253}LEDLRQQLQQAEEALVAKQELIDKLKEEAEQHKIV^{287}-NH_2) and sp-LZ in which the putative leucine zipper began at Leu^{315} (underlined) (^{294}LKAQADIYKADFQAERHAREKLVEKKEYLQEQLEQLQREFNKL^{336}-NH_2). In addition, a LZ peptide variant was synthesized with an N-terminal penetratin extension (underlined) and with an extra cysteine incorporated at the N terminus (CRQIKIWFQNRRMKWKKLKAQADIYKADFQAERHAREKLVEKKEYLQEQLEQLQREFNKL^{336}-NH_2). BODIPY®FL *N*-(2-aminoethyl)maleimide fluorophore (Molecular Probes) was conjugated to the SH group of its N-terminal cysteine in the presence of equimolar amounts of peptide and fluorophore in 50 mM ammonium acetate buffer, pH 6, for 30 min in the dark. The mixture was then loaded onto a Nucleoprep 20 μM C18 100-Å preparative column to remove free fluorophore. This BODIPY-labeled peptide was named Bp-LZ.

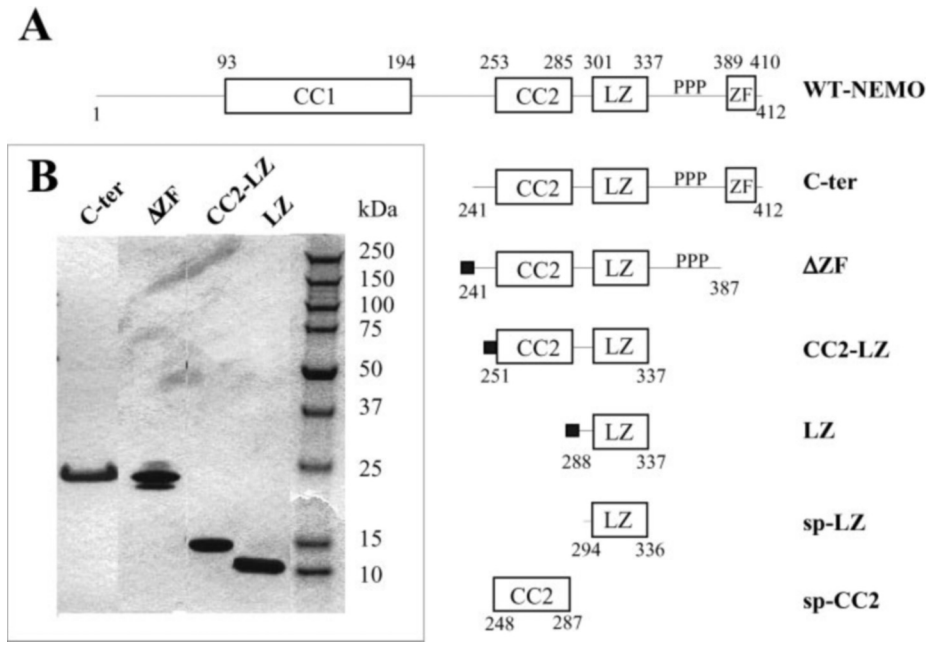

FIG. 2. **Recombinant proteins and synthetic peptides.** *A*, schematic representation of the wild-type NEMO protein (*WT-NEMO*), C-ter, and His-tagged (*black box*) recombinant proteins ΔZF, CC2-LZ, and LZ, as well as of the synthetic peptides sp-LZ and sp-CC2. The predicted coiled-coil (*CC*), leucine zipper (*LZ*), and zinc finger (*ZF*) motifs are indicated by *boxes*. *PPP*, proline-rich region. Amino acid numbering corresponds to the mouse NEMO protein. *B*, purification of the recombinant proteins. The SDS-PAGE gels were stained with Coomassie Blue. A molecular mass ladder is shown on the *right*.

Purification of Truncated Forms of NEMO Expressed in Escherichia coli—All truncated forms of NEMO were made by PCR mutagenesis using pRSETa/NEMO (1). Amplified fragments were digested with NheI and BamHI and cloned into pET-28b or pET-24a (Novagen). Recombinant Y241-E412 (C-ter), Y241-D387 (ΔZF), M251-K337 (CC2-LZ), and M288-K337 (LZ) proteins were verified by sequencing. All His-tagged truncated forms of NEMO contained a 23-residue N-terminal extension (MGSSHHHHHHSSGLVPRGSHMAS), including a site for proteolysis by thrombin (underlined). The C-ter devoid of the His tag, cloned in-frame into pET-24a, contained an extra two residues (Asp-Ser) at its N terminus. With the exception of C-ter, all proteins were produced at 37 °C. His-tagged ΔZF, CC2-LZ, and LZ were purified as in a previous study (1). C-ter was purified from a 2-liter culture of BL21(DE3) cells at 22 °C. The crude extract supernatant was treated with 100 μg of RNase (Roche Applied Science) and 3,500 units of DNase I from bovine pancreas (Roche Applied Science) for 30 min at 37 °C before loading on a Resource S column (6 ml, Amersham Biosciences) equilibrated in Buffer A (50 mM MES, pH 6.0, 0.2 mM DDM, 20 mM NaCl, and 1 mM dithioerythritol), and eluted with a 180-ml 20–1000 mM KCl linear gradient. Fractions containing C-ter NEMO protein according to SDS-PAGE were pooled and dialyzed against 1 liter of Buffer B (50 mM Tris-HCl, pH 8.0, 150 mM KCl, 0.2 mM DDM, and 1 mM dithioerythritol). The solution was then applied to a Resource Q column (6 ml, Amersham Biosciences) and the flow-through fractions containing the pure C-ter protein were pooled, concentrated by ultrafiltration (Millipore), and dialyzed extensively against Buffer B before freezing at −80 °C (1.4 mg/ml). Protein concentrations were determined by measuring $A_{280\ nm}$ and applying extinction coefficients calculated from their amino acid compositions: 0.142, 0.181, 0.184, and 0.278 unit·mg^{-1}·cm^2 for C-ter, ΔZF, CC2-LZ, and LZ polypeptides, respectively.

Gel Filtration Analysis—The oligomeric state and apparent Stoke's radius of recombinant proteins and synthetic peptides were determined after 15 h of preincubation at 20 °C by filtration of 500 μl samples on an analytical Superdex 75 column (Amersham Biosciences) equilibrated in 50 mM Tris-HCl, pH 8, buffer containing 200 mM sodium chloride, 0.1 mM DDM, and 1 mM dithioerythritol, developed at 0.5 ml/min. The void volume and the total volume of the column were measured with blue dextran 2000 and dithioerythritol, respectively. Protein elution was expressed as K_{av}. Depending on loading concentrations, sample elution was followed by measuring $A_{220\ nm/280\ nm}$ for sp-LZ or $A_{220\ nm/250\ nm}$ for sp-CC2. When necessary (see Fig. 5), peptides sp-LZ and sp-CC2 (200 μM each) were pre-mixed (20 min) in a denaturing buffer containing 20 mM Tris-HCl (pH 8.0), 4 M GdmCl, 150 mM KCl, and 1 mM DDM before loading on an analytical Superose 12 HR 10/30 column (Amersham Biosciences). The column was pre-equilibrated in 50 mM Tris-HCl (pH 8.0) containing 200 mM NaCl without GdmCl. Markers included bovine serum albumin (67 kDa, R_S = 35.2 Å), ovalbumin (43 kDa, R_S = 27.5 Å), chymotrypsinogen (25 kDa, R_S = 21.1 Å), ribonuclease A (13.7 kDa, R_S = 16.4 Å), cytochrome c (12.4 kDa, R_S = 17.1 Å), and aprotinin (6.5 kDa, R_S = 12.5 Å). In the case of LZ or sp-LZ, the equilibrium constant of the monomer/dimer equilibrium was determined by integrating the area of the elution peaks. The plot of the square of the monomer concentration *versus* dimer concentration (0.5–25 μM for LZ and 0.5–200 μM for sp-LZ) yielded a straight line, indicating that the system was at equilibrium. In the experiments with CC2-LZ-, ΔZF-, and C-ter-truncated forms of NEMO, the molar fraction of the trimer (x_{trimer}) at different loading concentrations was estimated according to the formula, $x_{trimer} = (K_{av}^{obs} - K_{av}^{monomer})/(K_{av}^{trimer} - K_{av}^{monomer})$, where K_{av}^{obs} is the partition coefficient of the monomer-trimer mixture at a given loading concentration, and $K_{av}^{monomer}$ and K_{av}^{trimer} are the partition coefficients of the monomer and trimer, respectively. Trimeric association constants were then estimated following the equation: $K_A = x_{trimer}/[3C_T^2(1 - x_{trimer})^3]$, where C_T is the total concentration of the monomeric species.

Sedimentation Equilibrium—Sedimentation equilibrium experiments were performed at 20 °C in a Beckman Optima XL-A analytical ultracentrifuge using an An 60-Ti rotor and three cells with two channel centerpieces. Sedimentation was carried out at 25,000, 35,000, 40,000, and 55,000 rpm with 120 μl of 15 μM or 35 μM sp-CC2 in 50 mM potassium phosphate buffer at pH 7.3. Lyophilized sp-CC2 was solubilized in phosphate buffer and allowed to equilibrate for 1 h at 20 °C prior to loading. Optical density was measured at 230 nm for optimal signal/background ratio. Equilibrium was verified by superimposing scans recorded at 2-h intervals. When equilibrium was reached, data were collected and centrifugation speed was increased to 55,000 rpm for 16 h to deplete the peptide concentration near the meniscus. The averaged data recorded around the top of the cell were then taken as zero and offset to obtain a baseline correction of the cell. The $\bar{\nu}$ of sp-CC2, calculated from its amino acid composition, was 0.746 ± 0.005 ml/g, and the calculated density of the buffer was 1.005 g/ml at 20 °C (29). Data were fitted with one, two, or multispecies models as described previously (30, 31). Inclusion of a second virial coefficient never improved the fit.

Fluorescence Anisotropy—Anisotropy was measured with a PTI Quantamaster fluorometer equipped with polarizers for the excitation and emission beams using a photomultiplier tube in the L-configuration. All experiments were carried out in a 1-cm path length cuvette at 22 °C with excitation and emission wavelengths of 495 nm and 520 nm, respectively. The bandpasses of the excitation and emission monochromators were set at 2 and 4 nm, respectively. Steady-state fluorescence anisotropy, expressed in millianisotropy units, was calculated according to the equation, $A = (I_{VV} - GI_{VH})/(I_{VV} + 2GI_{VH})$, where A is anisotropy, $G = I_{HV}/I_{HH}$ is a correction factor for wavelength-dependent distortion, and I is the fluorescence intensity component. Experiments were performed at least twice, and each point is the result of 20 recordings taken during a 2-min period. All measurements were carried out in 50 mM Tris-HCl buffer at pH 8 containing 150 mM KCl. We verified that the filter effect was negligible at the Bp-LZ concentration used (0.1 μM). The Bp-LZ peptide was preincubated at 22 °C alone or with increasing concentrations (1–125 μM) of sp-CC2 prior to anisotropy readings. The dissociation constant was estimated by fitting the anisotropy data to the binding isotherm equation

using Kaleidagraph non-linear regression software (Synergy Software, Reading PA) as described previously (32).

RESULTS

Both the CC2 and LZ Domains Are Essential to Restore LPS-induced NF-κB Activity in NEMO-deficient 1.3E2 Cells—The murine pre-B cell mutant 1.3E2 not expressing NEMO does not respond to LPS activation (6, 26). These cells were transiently co-transfected with an NF-κB-dependent construct (Igκ-luciferase) and plasmids bearing wild-type or mutant *nemo* cDNAs. When mock co-transfected with an empty vector and the reporter plasmid, the cells remained non-responsive (Fig. 1*A*, *lane 1*). Unlike when co-transfected with the wild-type *nemo* gene (Fig. 1*A*, *lane 2*), cells did not recover LPS-dependent luciferase activity when transfected with a *nemo* cDNA deleted of the region coding for part of the CC2 domain (Fig. 1*A*, *lane 3*). The LZ domain is predicted to form a coiled-coil motif with the hydrophobic residues of the heptad repeat located at the coiled-coil interface (33). Thus, the substitution of Leu^{322} and Leu^{329}, which are located at these positions by polar residues (Ser), is likely to destabilize the LZ coiled-coil interactions. Indeed, the L322S/L329S mutant of the LZ domain was also not responsive (Fig. 1*A*, *lane 4*). Stable transfections with wild-type *nemo* or with mutant *nemo* cDNAs were also performed. The nuclear extracts were analyzed by a gel retardation assay after LPS stimulation. Transfection with a plasmid coding for the L322S/L329S mutant (Fig. 1*B*, EMSA, *lane LZ Mut*) generated considerably less DNA-binding activity than transfection with wild-type *nemo* cDNA (Fig. 1*B*, EMSA, *lane WT*) or in the parental 70Z/3 cells (Fig. 1*B*, EMSA, *lane 70Z/3*). As shown by Western blots, the level of the proteins was similar in the parental 70Z/3 cells and in transfected 1.3E2 cells (Fig. 1*B*, *WB*), ruling out the possibility that the pathway was inhibited by overexpression of mutant HA-NEMO.

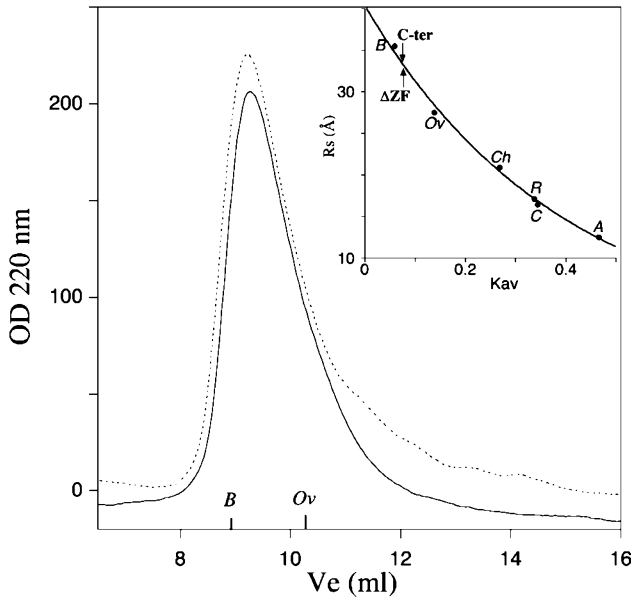

FIG. 3. **Gel filtration analysis of the ΔZF protein.** *Solid line*: C-ter protein; *dotted line*: ΔZF protein. The elution volumes (V_e) of bovine serum albumin (*B*) and of ovalbumin (*Ov*) are indicated. *Inset*, calibration curve for marker proteins measured in the same experimental conditions. The K_{av} of the C-ter and ΔZF recombinant proteins are indicated by *arrows*. *Ch*, chymotrypsinogen; *R*, ribonuclease A; *C*, cytochrome c; *A*, aprotinin.

Purification of Recombinant NEMO Subdomains Expressed in E. coli—Fig. 2*A* shows the C-ter protein of the His-tagged recombinant NEMO construct and the synthetic peptides corresponding to the various domains of the C-terminal half of NEMO used in this study. All NEMO subdomain constructs (ΔZF, CC2-LZ, and LZ) were expressed as soluble proteins in *E. coli* at 37 °C, with the exception of the C-ter protein, which had to be produced at 22 °C to obtain a soluble protein. The minor component of the ΔZF doublet corresponds to a proteolyzed protein as shown by Western blots using anti-His tag and anti-NEMO C-ter antibodies and by matrix-assisted laser desorption ionization time-of-flight mass spectrometry (data not shown). The apparent molecular weights of the four recombinant fragments purified to homogeneity (Fig. 2*B*) were in agreement with their calculated molecular weights.

Role of C-terminal Subdomains in NEMO Oligomerization—The ΔZF-truncated protein (241–387) was compared with the entire C-ter protein by size exclusion chromatography. Both proteins co-eluted when loaded at 10 μM (Fig. 3). The K_{av}, estimated by comparison with the R_S (Å) of standard globular proteins (*inset*, Fig. 3), was consistent with the presence of trimeric species. However, the width of the peaks suggested an equilibrium with dissociated forms. We thus performed a series of experiments at various ΔZF concentrations (0.1–10 μM) (not shown) to study variations in the monomer/trimer ratio. This gave a K_A of $0.5 \pm 0.2 \times 10^9$ M^{-2} (Table I), which was almost identical to that previously determined by sedimentation equilibrium for the C-ter domain ($1.5 \pm 0.7 \times 10^9$ M^{-2}) (1). This value was also confirmed by sedimentation equilibrium (not shown). These results demonstrate that the ZF motif of NEMO is not involved in NEMO self-assembly.

We next deleted the proline-rich region (PPP) between the LZ and the ZF motifs (see Fig. 2), along with the first 10 residues of the C-ter domain (amino acids 241–250), yielding the CC2-LZ recombinant protein (amino acids 251–337). The elution profile of gel filtration experiments performed at various loading concentrations was monomodal even at a low concentration (0.5 μM) (Fig. 4*A*). The slight shift in the peak at the

TABLE I

Oligomerization state of NEMO recombinant proteins and of synthetic peptides

The oligomeric state of the NEMO recombinant proteins and of synthetic peptides sp-LZ and sp-CC2 is indicated. The K_A of the monomer/trimer and of the monomer/dimer equilibria, as well as the corresponding free energy of binding ($\Delta G°$) of the reaction at 20 °C are given for each of the polypeptides.

Protein or synthetic peptide (sp)	Oligomeric state	K_A		$\Delta G°$
		Monomer-trimer	Monomer-dimer	
		M^{-2}	M^{-1}	$kcal \cdot mol^{-1}$
C-ter	Trimer[a]	$1.5 \pm 0.7 \times 10^9$		-12.3 ± 0.3
ΔZF	Trimer[b]	$0.5 \pm 0.2 \times 10^9$		-11.7 ± 0.2
CC2-LZ	Trimer[c]	$0.8 \pm 0.4 \times 10^9$		-11.9 ± 0.3
LZ	Dimer[c]		$9 \pm 5 \times 10^4$	-6.6 ± 0.3
sp-LZ	Dimer[c]		$6 \pm 4 \times 10^4$	-6.4 ± 0.4
sp-CC2	Trimer[a]	$3.3 \pm 0.5 \times 10^7$		-10.0 ± 0.1

[a] Values calculated from both gel filtration and sedimentation equilibrium experiments.
[b] Data calculated from sedimentation equilibrium experiments taken from Ref. 1.
[c] Values calculated from gel filtration experiments.

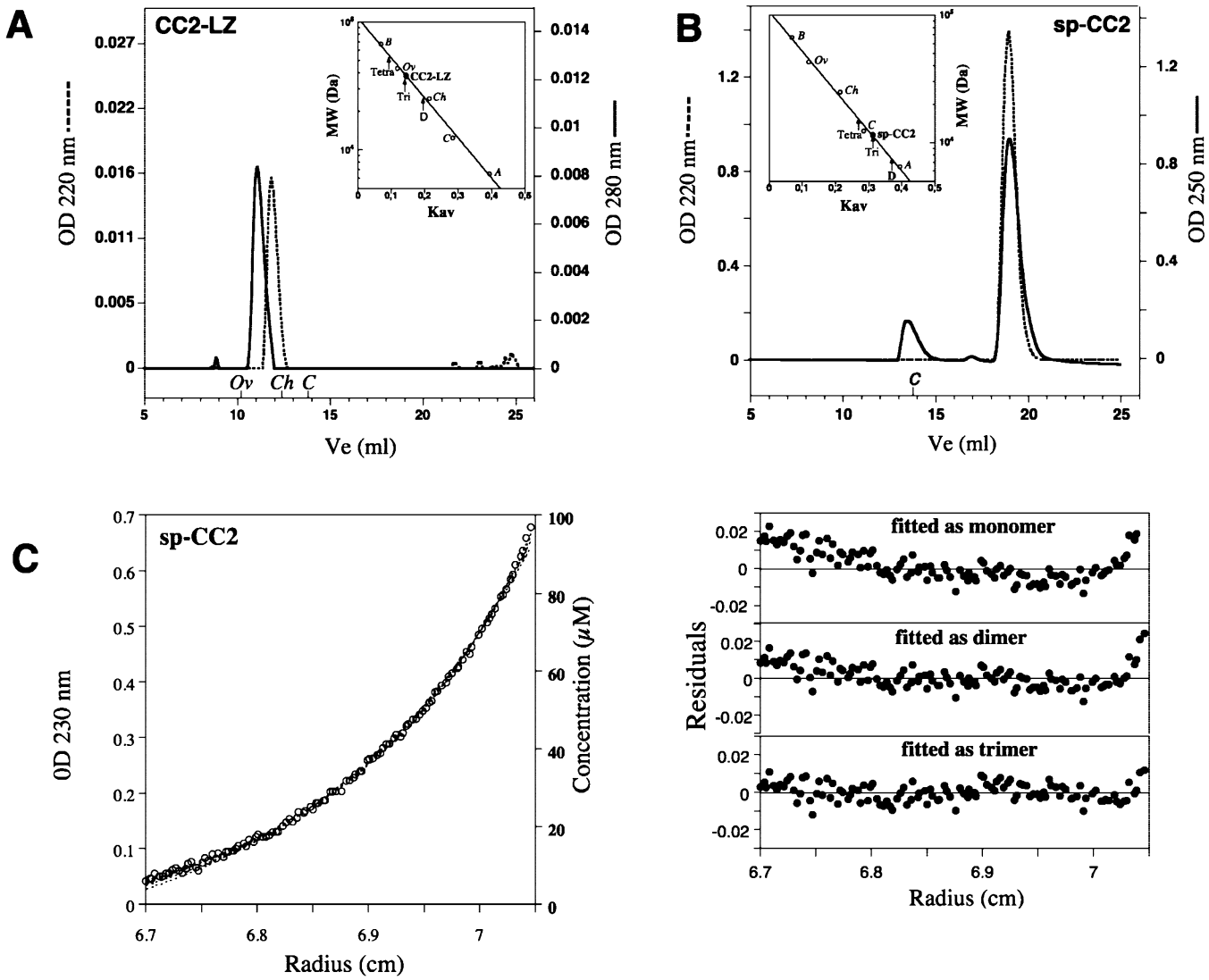

FIG. 4. **Analysis of the oligomerization state of the CC2-LZ protein and of sp-CC2.** *A* and *B*, exclusion chromatography. Elution profiles of CC2-LZ recombinant protein (*A*) and of the sp-CC2 peptide (*B*) on a Superdex 75 HR 10/30 column. The concentrations of the injected samples were 15 μM (*solid line*) or 0.5 μM (*dotted line*) for CC2-LZ, and 100 μM (*solid line*) or 2 μM (*dotted line*) for sp-CC2. The low and high CC2-LZ protein concentrations were detected at 220 and 280 nm, respectively. The low and high sp-CC2 concentrations were detected at 220 and 250 nm, respectively. The elution volume of standard proteins is shown on the abscissa. *Insets*, the log of the molecular mass (Da) of marker proteins is plotted against K_{av}. K_{av} values of CC2-LZ and of sp-CC2 are indicated by a *black circle*. The theoretical positions of the tetrameric (*Tetra*), trimeric (*Tri*), and dimeric (*D*) forms of the corresponding peptides are also indicated. *C*, analysis of sp-CC2 by sedimentation equilibrium. The sedimentation profile of CC2 (35 μM) measured by its absorbance at 230 nm is plotted as a function of radial distance at 35,000 rpm (*left panel*). The sedimentation data were fitted using a mono-species model (monomer) and a two-species model (dimer or trimer) as indicated in the *right panel*. The *line* shows the best-fitting curve for an ideal two-species model corresponding to the monomer/trimer equilibrium.

low concentration suggests minor dissociation. At the high concentration, the K_{av} was 0.143 (Fig. 4*A*, *inset*), corresponding to a molecular mass of 39 kDa, which is similar to the theoretical molecular mass of the trimer (38.61 kDa). The estimated K_A for the monomer/trimer equilibrium was $0.8 \pm 0.4 \times 10^9$ M^{-2} (Table I).

To analyze the contribution of each subdomain in the self-association of CC2-LZ, we analyzed the oligomeric structure of the two synthetic peptides (sp-CC2 and sp-LZ). Unlike the CC2-LZ recombinant protein, gel filtration of sp-CC2 generated two major peaks in a concentration-dependent ratio (Fig. 4*B*). The heavier species, corresponding to the trimeric form, eluted at 13.5 ml (R_S = 17.7 Å), and the major peak, corresponding to the monomer, was lighter (calculated mass 4.1 kDa).

The oligomeric state of sp-CC2 was also analyzed by sedimentation equilibrium. All radial distributions at 25,000, 35,000, 40,000, and 55,000 rpm with loading concentrations of either 15 or 35 μM were not highly consistent with a single species model or a monomer/dimer model (Fig. 4*C* and Table II). The average calculated molecular weight was intermediate between monomeric and trimeric species, most consistent with a monomer-trimer equilibrium. The use of a three-component model (monomer-dimer-trimer) or a tetramer model did not

TABLE II
Sedimentation equilibrium of the sp-CC2 peptide

The average molecular mass was calculated by fitting to a model for a single ideal species. χ^2 is the weighted sum of squared residuals.

Initial peptide concentration	Speed	Single species	χ^2	Monomer-trimer equilibrium	χ^2
μM	rpm	Da		K_A ($\times 10^{-7}$ M^{-2})	
35	25 000	6600 ± 300	20	2 ± 1	18
35	35 000	6550 ± 200	54	1.3 ± 0.2	40
35	55 000	6250 ± 200	263	1.3 ± 0.1	90
15	40 000	5800 ± 200	62	3.5 ± 0.7	50
15	55 000	5300 ± 150	60	5 ± 2	35

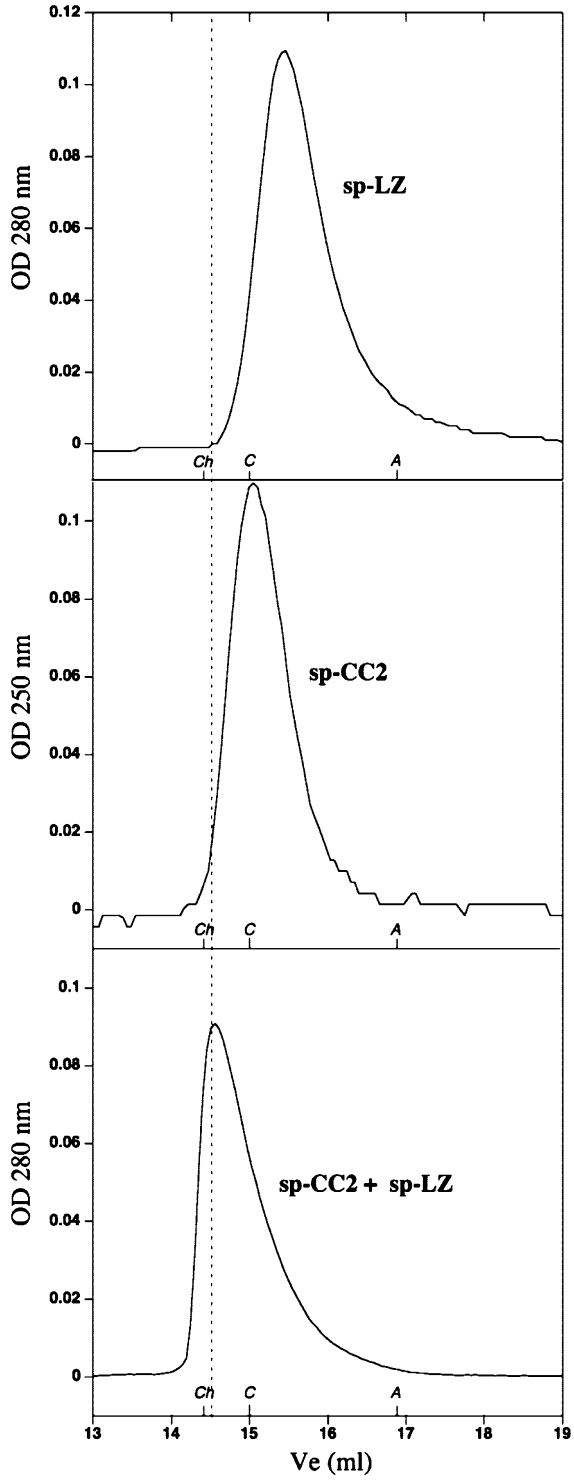

FIG. 5. **Interaction between sp-CC2 and sp-LZ peptides: gel filtration.** Peptides (200 μM) were loaded on an analytical Superose 12 HR 10/30 column. Elution volumes were 15.7 ml for sp-LZ, 15.2 ml for sp-CC2, and 14.5 ml for an equimolar mixture of sp-CC2 and of sp-LZ (sp-CC2 plus sp-LZ). sp-CC2 was detected at 250 nm, and sp-LZ peptide at 280 nm. The elution volume of markers is shown as in Fig. 4.

improve the fit. The concentration and speed dependence of the K_A for the monomer-trimer equilibrium were very similar (Table II), indicating that the equilibrium was reversible. When these data were merged and fitted at four different speeds, they gave a K_A of 3.3 $\pm$ 0.5 $\times$ 10^7 M^{-2} for the monomer/trimer association of sp-CC2, a value 25-fold lower than for the CC2-LZ recombinant protein (Table I).

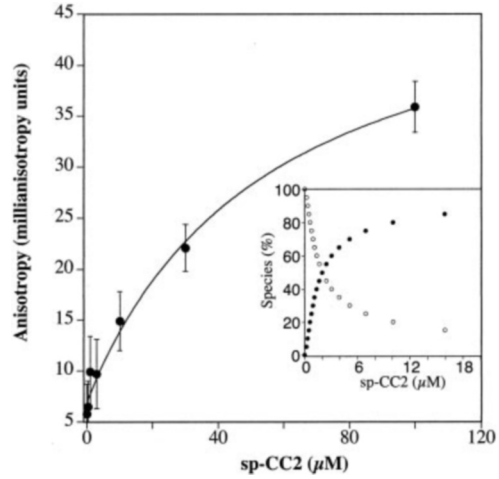

FIG. 6. **Titration of Bp-LZ with sp-CC2 by fluorescence anisotropy.** BODIPY-labeled Bp-LZ (0.1 μM) was used as a probe. The concentration of sp-CC2 was determined by amino acid analysis. Anisotropy values of Bp-LZ in milliunits (millianisotropy units) were plotted against sp-CC2 concentration. Data points were fitted to the binding isotherm equation (*solid line*) with a K_D of 55 μM. *Inset*, distribution of trimeric (*black circles*) and monomeric (*open circle*) species as a function of the total concentration of sp-CC2 as deduced from the sedimentation equilibrium data (Fig. 4*C*).

A similar analysis was performed to investigate the oligomeric state of sp-LZ (data not shown). Again, the peptide eluted in two peaks, but whereas the second one also corresponded to the monomer, the first peak corresponded to a dimer, with a K_A of 6 $\pm$ 4 $\times$ 10^4 M^{-1} for the monomer-dimer equilibrium. The behavior of the His-tagged LZ recombinant polypeptide was similar to that of the synthetic sp-LZ peptide with a K_A of 9 $\pm$ 5 $\times$ 10^4 M^{-1} for the monomer-dimer equilibrium (Table I) (data not shown), indicating that the His tag does not interfere with LZ dimerization.

The LZ Domain Binds to the CC2 Domain—The fact that the monomer/trimer K_A was higher for CC2-LZ than for sp-CC2 suggested that LZ is involved in the oligomerization of NEMO. This hypothesis was tested by performing mixing experiments, followed by gel filtration. The aromatic-free sp-CC2 was monitored at 250 nm, whereas sp-LZ was specifically monitored at 280 nm. The peptides were first preincubated with 4 M GdmCl to destroy their quaternary structure and were then loaded alone or after mixing onto a column equilibrated in guanidine-free buffer. In these conditions, sp-CC2 and sp-LZ re-associate as trimers and dimers, respectively (Fig. 5). In contrast, upon mixing with sp-CC2, the sp-LZ peptide co-eluted with chymotrypsinogen (25 kDa), indicating an association with sp-CC2. The elution of this complex corresponds to the theoretical elution of a heterohexamer composed of three sp-CC2 peptides associated with three sp-LZ peptides (theoretical molecular mass = 28.2 kDa). Because the complex was monitored at 280 nm, its elution as a single peak indicates that most sp-LZ peptides were associated with sp-CC2. Moreover, the absence of a peak at the position corresponding to the sp-CC2 trimer when the elution was monitored at 220 nm (not shown), probably indicates that sp-CC2 was totally titrated by sp-LZ in a 1:1 stoichiometry.

The ability of sp-CC2 to bind to sp-LZ was also analyzed by fluorescence anisotropy. For this, we used a modified sp-LZ peptide in which the N-terminal cysteine was linked to a BODIPY fluorescent dye. Titration of this Bp-LZ peptide with increasing concentrations of sp-CC2 resulted in a gradual increase in fluorescence anisotropy, reaching seven times the basal value at 100 μM sp-CC2 (Fig. 6). The binding curve was not sigmoidal, indicating the lack of cooperativity of the inter-

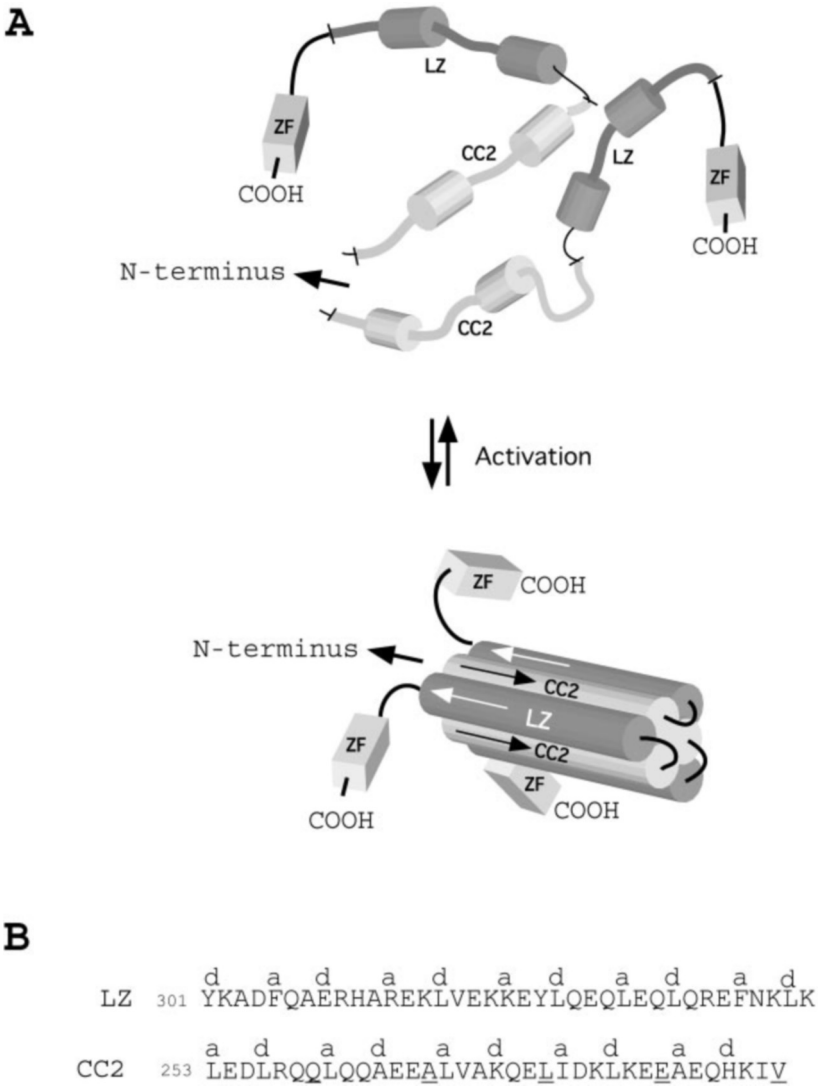

FIG. 7. **A model for the C-terminal domain of NEMO.** *A*, α-helices in CC2 (*light gray*) and LZ (*dark gray*) are represented as *rods* and the ZF motif by a *square rod*. In the relaxed C-ter domain (*top*), the native CC2 and LZ subdomains are disordered with a low α-helix content. In the trimeric form (*bottom*), the LZ helices dock in the crevices defined by the external interfaces of a central core CC2 made of three coiled-coils to form a six-helix bundle. In this configuration, both the CC2 and LZ subdomains are depicted by longer helices to indicate their induced structure formation. *B*, sequences of the CC2 and LZ coiled-coil subdomains showing the "*a*" and "*d*" positions of the heptad repeats. The amino acids in the "*g*" positions of the CC2 heptad repeats are *underlined*.

action. When the data were fitted to a simple binding model a dissociation constant of 55 μM was obtained for sp-CC2 to Bp-LZ with a stoichiometry of one Bp-LZ per sp-CC2. The fact that the amount of the heterocomplex paralleled the amount of sp-CC2 trimers deduced by sedimentation equilibrium (Fig. 6, *inset*) strongly suggests that LZ binds preferentially to the trimeric form of sp-CC2.

DISCUSSION

NEMO/IKKγ is a non-redundant element of the IKK complex that connects a wide variety of extracellular signals to several important downstream intracellular cascades. In this report, we focused on the study of the C-terminal half of NEMO (also called C-ter), which is involved both in signal perception and in the oligomerization of the protein. We purified several NEMO subdomains as recombinant proteins or as synthetic peptides (see Fig. 2) and analyzed their functional and structural properties. Functional complementation of a NEMO-deficient cell line demonstrated that both CC2 and LZ domains are required for the activation of the NF-κB pathway (Fig. 1). NEMO was inactivated by deleting part of the CC2 motif or by creating a L322S/L329S double mutation in the LZ motif. Interestingly, a L322P mutation in the LZ subdomain also abolished phenotypic rescue of the pathway in MEF cells (34). We hypothesize that this mutation disorganizes the LZ α-helix, whereas the Leu-Ser substitutions probably alter the interfaces of the coiled-coil interactions between CC2 and LZ domains within the oligomer.

There is much evidence suggesting that NEMO self-associates (see the introduction). Because zinc finger domains, which perform a wide range of functions in cellular processes (see Ref. 35 for a review), are also implicated in protein dimerization, the crucial role of the ZF domain in NEMO function could be linked to its role in oligomerization. Here, we demonstrate that this is not the case, because deletion of the ZF subdomain had no effect on the Stoke's radius of the protein, whether measured by gel filtration (this work, Fig. 3) or by sedimentation equilibrium (1).

Our experiments show that both ΔZF and CC2-LZ recombinant proteins form trimers with very similar K_A to the entire C-ter domain (Table I). Although CC2-LZ represents only 50% of the length of the C-ter, it accounts for 97% of the $\Delta G°$ of its association in trimers, indicating that it contains all of the amino acids involved in NEMO oligomerization. These results reduce the size of the minimal oligomerization domain to 87 residues (amino acids 251–337). Our observation that full-length NEMO (1) and either CC2-LZ or the isolated CC2 subdomain (this report) all form trimeric oligomers is in agreement with other studies (7, 20). Tegethoff *et al.* (21) proposed that the minimal oligomerization domain has a tetrameric structure. There are several possible explanations for this discrepancy: (i) their cross-linking experiments were performed using crude

cell lysates and high concentrations (5 mM) of a cross-linker (ethylene glycol-bissuccinimidylsuccinate) known to react with SH and NH_2 groups, possibly resulting in nonspecific cross-links between NEMO polypeptides and/or heterologous proteins, and (ii) the absence of a reducing agent in the buffer used in sedimentation equilibrium experiments, which could similarly induce the formation of illegitimate disulfide bonds. Finally, the molecular weight of the protein may have been overestimated due to the lack of a spectrophotometer zero offset needed to perform baseline corrections in the centrifugation experiments (30).

Whatever the reasons for these discrepancies, it should be emphasized that a relationship between the hydrodynamic properties of NEMO and its apparent molecular weight could be misleading. Indeed, the hydrodynamic properties of the C-ter domain alone markedly differ from those of full-length NEMO. Although the C-ter trimer behaves as a globular domain, full-length NEMO displays a large 73 Å Stoke's radius along with a small 4.1 S sedimentation coefficient, typical of an elongated protein (1, 36). Therefore, the chromatographic behavior of NEMO overexpressed in different cell lines should be analyzed carefully as a molecular mass of ~550 kDa for the free form of NEMO is close to that of the IKK complex (~700 kDa) (37). This abnormal chromatographic behavior may also explain why no change in the oligomeric state of NEMO could be detected upon stimulation of cells with pro-inflammatory signals (37).

To elucidate the contribution of each subdomain in the building of the NEMO oligomer, we analyzed the oligomeric structure of isolated CC2 and LZ subdomains. Sp-CC2 was eluted as a trimer upon gel filtration (Fig. 4*B*), with an association constant ~25-fold weaker than that of CC2-LZ polypeptide (Table I). In contrast, the LZ subdomain (both the recombinant protein and the synthetic peptide) formed dimers with an association constant of $\sim 10^5\ M^{-1}$ (Table I). The question then arises of a possible hetero-association between the CC2 and LZ domains within the same polypeptide. When sp-CC2 and sp-LZ were mixed after denaturation to disrupt their quaternary structure, the peptides associated into a hexameric complex with the hydrodynamic properties of a globular protein (Fig. 5). The association constant of this complex was high, as indicated by the fact that most of the sp-LZ was titrated by sp-CC2. The direct interaction between sp-LZ and sp-CC2 was further demonstrated by fluorescence polarization experiments (Fig. 6). The increase in Bp-LZ anisotropy in the presence of increasing concentrations of sp-CC2 correlates with the formation of sp-CC2 trimers, suggesting that sp-LZ preferentially associates with the trimeric form of CC2.

Our results propose a model for the structural organization of the minimal oligomerization domain of NEMO (Fig. 7*A*). The main feature of this model is the docking of LZ α-helices in the crevices defined by two of the helices of the central trimeric CC2 coiled-coil domain, forming a pseudo-hexameric six-helix bundle. This model takes into account all of the known biochemical properties of NEMO oligomerization. The presence of unusual hydrophobic residues in the "g" position of the heptad repeat of the CC2 coiled-coil (Fig. 7*B*) could explain the requirement for DDM detergent to improve the yield of sp-CC2 in gel filtration at millimolar concentrations. We speculate that the LZ domain protects these hydrophobic residues from solvent exposure. Considering the short linker between CC2 and LZ motifs, we predict an anti-parallel orientation. Note that a proline is present in the connecting loop, possibly contributing to bending.

Given its external position, the LZ motif, alone or in combination with the ZF motif, could allow interactions between the oligomerization domain and upstream activators. For example, receptor-interacting protein promotes IKK activation by changing NEMO structure (18). Our model also provides an explanation for the previously observed concentration dependence of the C-ter domain helicity (1). Indeed, the establishment of specific coiled-coil contacts between CC2 and LZ subdomains is likely to result in the fully-folded conformation of the oligomerization domain, thus increasing its helicity (see Fig. 7*A*). A similar case was described in the transition between the native and post-fusogenic states of type I viral proteins (38). The similarity between the proposed structure of the NEMO oligomerization domain and the ectodomain of HIV-1 gp41 (39) is noteworthy.

We propose that, in the resting state, the C-ter domain of NEMO is natively disordered (Fig. 7*A*, *upper part*) as are members of the "disordered proteins" family (40). This could confer functional advantages to NEMO by enhancing its binding capacity to activators and/or allowing its binding to multiple activators. We speculate that, following cell stimulation, the binding of an upstream activator to NEMO promotes its fully-folded state and induces the formation of the six α-helix bundle, a process that may be reliant on the ZF motif. The mechanism by which this conformational change activates the IKK complex remains unclear.

The crucial role played by the interactions between CC2 and LZ motifs in NEMO oligomerization and thus in NF-κB activation suggests that these subdomains could provide therapeutic targets to inhibit the NF-κB pathway *in vivo*. We are currently investigating the inhibitory properties of permeable peptides designed to block the NF-κB pathway specifically by disrupting NEMO oligomerization.

Acknowledgments—We thank Dr. F. Baleux and Y. M. Coïc (Unité de Chimie Organique, Institut Pasteur) for peptide synthesis, Dr. R. Weil for helpful discussions, Dr. E. Fontan for critical reading of the manuscript, and all members of the team "systèmes et réseau" at the Pasteur Institute. The excellent technical assistance of S. Goffinont and the help of D. Müller during part of this work are gratefully acknowledged.

REFERENCES

1. Agou, F., Ye, F., Goffinont, S., Courtois, G., Yamaoka, S., Israël, A., and Véron, M. (2002) *J. Biol. Chem.* **277,** 17467–17475
2. Bauerle, P. A., and Baltimore, D. (1996) *Cell* **87,** 13–20
3. Ghosh, S., May, M. J., and Kopp, E. B. (1998) *Annu. Rev. Immunol.* **16,** 225–260
4. Karin, M., and Ben-Neriah, Y. (2000) *Annu. Rev. Immunol.* **18,** 621–663
5. Courtois, G., Smahi, A., and Israël, A. (2001) *Trends Mol. Med.* **7,** 427–430
6. Yamaoka, S., Courtois, G., Bessia, C., Whiteside, S. T., Weil, R., Agou, F., Kirk, H. E., Kay, R. J., and Israël, A. (1998) *Cell* **93,** 1231–1240
7. Rothwarf, D. M., Zandi, E., Natoli, G., and Karin, M. (1998) *Nature* **395,** 297–300
8. Zandi, E., Rothwarf, D. M., Delhase, M., Hayakawa, M., and Karin, M. (1997) *Cell* **91,** 243–252
9. Makris, C., Godfrey, V. L., Krähn-Senftleben, G., Takahashi, T., Roberts, J. L., Schwartz, T., Feng, L., Johnson, R. S., and Karin, M. (2000) *Mol. Cell. Biol.* **15,** 969–979
10. Rudolph, D., Yeh, W.-C., Wakeham, A., Rudolph, B., Nallainathan, D., Potter, J., Elia, A. J., and Mak, T. W. (2000) *Genes Dev.* **14,** 854–862
11. Zandi, E., Chen, Y., and Karin, M. (1998) *Science* **281,** 1360–1363
12. Prajapati, S., and Gaynor, R. B. (2002) *J. Biol. Chem.* **277,** 24331–24339
13. Tang, E. D., Wang, C. Y., Xiong, Y., and Guan, K. L. (2003) *J. Biol. Chem.* **278,** 37297–37305
14. Brummelkamp, T. R., Nijman, S. M., Dirac, A. M., and Bernards, R. (2003) *Nature* **424,** 797–801
15. Trompouki, E., Hatzivassilou, E., Tsichritzis, T., Farmer, H., Ashworth, A., and Mosialos, G. (2003) *Nature* **424,** 793–796
16. Kovalenko, A., Chable-Bessia, C., Cantarella, G., Israël, A., Wallach, D., and Courtois, G. (2003) *Nature* **424,** 801–805
17. Inohara, N., Koseki, T., Lin, J., del Peso, L., Lucas, P. C., Chen, F. F., Ogura, Y., and Nunez, G. (2000) *J. Biol. Chem.* **275,** 27823–27831
18. Poyet, J.-L., Srinivasula, S. M., Lin, J.-H, Fernandes-Alnmeri, T., Yamaoka, S., Tsichlis, P. N., and Alnemri, E. S. (2000) *J. Biol. Chem.* **275,** 37966–37977
19. Poyet, J.-L., Srinivasula, S. M., and Alnemri, E. S. (2001) *J. Biol. Chem.* **276,** 3183–3187
20. Huang, G.-J., Zhang, Z. Q., and Jin, D. Y. (2002) *FEBS Lett.* **531,** 494–498
21. Tegethoff, S., Behlke, J., and Sheidereit, C. (2003) *Mol. Cell. Biol.* **23,** 2029–2041
22. Huang, T. T., Feinberg, S. L., Suryanarayanan, S. and Miyamoto, S. (2002) *Mol. Cell. Biol.* **22,** 5813–5825

23. Smahi, A., Courtois, G., Vabres, P., Yamaoka, S., Heuertz, S., Munnich, A., Israel, A., Heiss, N. S., Klauck, S. M., Kioschis, P., Wiemann, S., Poustka, A., Esposito, T., Bardaro, T., Gianfrancesco, F., Ciccodicola, A., D'Urso, M., Woffendin, H., Jakins, T., Donnai, D., Stewart, H., Kenwrick, S. J., Aradhya, S., Yamagata, T., Levy, M., Lewis, R. A., and Nelson, D. L. (2000) *Nature* **405,** 466–472
24. Döffinger, R., Smahi, A., Bessia, C., Geissman, F., Feinberg, J., Durandy, A., Bodemer, C., Kenwrick, S., Dupuis-Girod, S., Blanche, S., Wood, P., Rabia, S. H., Headon, D. J., Overbeek, P. A., Le Deist, F., Holland, S., Belani, K., Kumararatne, D. S., Fisher, A., Shapiro, R., Conley, M. E., Reimund, E., Kalhoff, H., Abinun, M., Munnich, A., Israël, A., Courtois, G. and Casanova, J.-L. (2001) *Nat. Genet.* **27,** 277–285
25. Jain, A., Ma, C. A., Liu, S., Brown, M., Cohen, J., and Strober, W. (2001) *Nat. Immunol.* **2,** 223–228
26. Courtois, G., Whiteside, S. T., Sibley, C. H., and Israël, A. (1997) *Mol. Cell. Biol.* **17,** 1441–1449
27. Chan, W. C., and White, P. D. (2000) *Fmoc Solid-Phase Peptide Synthesis. A Practical Approach*, Oxford University Press, Oxford, UK
28. Mousson, F., Beswick, V., Coic, Y.-M., Baleux, F., Huynh-Dinh, T., Sanson, A., and Neumann, J.-M. (2002) *Biochemistry* **41,** 13611–13616
29. Laue, T. M., Bhaivari, D. S., Ridgeway, T. M., and Pelletier, S. L. (1992) in *Analytical Ultracentrifugation in Biochemistry and Polymer Science* (Harding, S. E., Rowe, A. J., and Horton, J. C., eds) pp. 90–125, Royal Society of Chemistry, Cambridge, UK
30. Johnson, M., and Straume, M. (1994) in *Modern Analytical Ultracentrifugation* (Schuster, T. M., and Laue, T., eds) pp. 37–65, Birkhauser Boston, Inc. Cambridge, MA
31. Agou, F., Waller, J. P., and Mirande, M. (1996) *J. Biol. Chem.* **271,** 29295–29303
32. Agou, F., Raveh, S., Mesnildrey, S., and Veron, M. (1999) *J. Biol. Chem.* **274,** 19630–19638
33. Vinson, C., Myakishev, M., Acharya, A., Mir, A. A., Moll, J. R., and Bonovich, M. (2002) *Mol. Cell. Biol.* **22,** 6321–6335
34. Makris, C., Roberts, J. L., and Karin, M. (2002) *Mol. Cell. Biol.* **22,** 6573–6581
35. Krishna, S. S., Majumdar, I., and Grishin, N. V. (2003) *Nucleic Acids Res.* **31,** 532–550
36. Siegel, M., and Monty, K. J. (1965) *Biophys. Res. Commun.* **19,** 494–499
37. Li, X.-H., Fang X., and Gaynor, R. B. (2001) *J. Biol. Chem.* **276,** 4494–4500
38. Colman, P. M., and Lawrence, M. C. (2003) *Nat. Rev. Mol. Cell. Biol.* **4,** 309–319
39. Chan, D. C., Fass, D., Berger, J. M., and Kim, P. S. (1997) *Cell* **89,** 263–273
40. Gunasekaran, K., Tsai, C.-J., Kumar, S., Zanuy, D., and Nussinov, R. (2003) *Trends Biochem. Sci.* **28,** 81–85